Clinical Evaluation of Somatostatin Use in Pancreatic Resections: Clinical Efficacy or Limited Benefit?

Ryan Anderson, BS, Erik Dunki-Jacobs, MD, Charles Scoggins, MD Kelly McMasters, MD, PhD
Glenda Callender, MD, Nicolas Burnett, BA, Robert CG Martin II, MD, PhD
Department of Surgery, Division of Surgical Oncology, University of Louisville School of Medicine

Introduction

- Pancreatic cancer is the fourth leading cause of cancer death in the United States and has a five year survival rate of less than five percent.
- The number of pancreatectomies performed each year has increased with mortality decreasing to acceptable over the past 10 – 20 years.
- However, morbidity remains high.
- Contemporary reviews cite post-operative morbidity at 30% – 60%, with pancreatic fistula being the most common morbidity at 5% – 30%.
- Pancreatic fistula is one of the most morbid and costly complications associated with pancreatectomy.
- Many strategies, both technical and pharmacological, have been put forth to attenuate this morbidity, but no consensus for treatment has been reached

Purpose of Study

- Evaluate the efficacy of somatostatin in preventing pancreatic fistulas and improving post-surgical outcomes after pancreatic resection.

Methods

- A review of a prospectively collected hepato-pancreatico-biliary database was performed.
- Patients were included if the underwent pancreatectomy between 10/01/91 and 05/16/2012.
- Patients received somatostatin prophylactically at the discretion of their surgeon.
- Data were analyzed using univariate and multivariate analysis to determine if somatostatin had any effect on pancreatic fistula formation, fistula severity, length of stay (LOS), and readmission rates.

Results

Characteristic	N= 510 (%)
Age (median, range)	63 (15-92)
Gender	
Male	258 (51%)
Female	252 (49%)
BMI (median,range)	26 (13-52)
<=18.5	18 (4%)
25+	291 (57%)
30+	44 (9%)
Pancreatic Fistula/Leak	30 (6%)
A	3 (1%)
B	13 (3%)
C	14 (3%)
B and C	27 (5%)
PMH	
Cardiac	121 (24%)
Pulmonary	62 (12%)
Diabetes	104 (20%)
Alcohol	66 (13%)
Tobacco	179 (35%)
Hepatic	14 (3%)
Pancreatitis	19 (4%)
PSH	
Cholecystectomy	105 (21%)
Colectomy	21 (4%)
Appendectomy	38 (8%)
LOS (median, range)	9 (2-81)
Somatostatin administered	215 (42%)
Whipple	389 (76%)
Distal Pancreatectomy	121 (24%)
Readmission	57 (11%)
Pre-operative Chemo	3 (1%)

Table 1. Clinicopathological data on all 510 patients undergoing pancreatectomy between 10/01/91 and 05/16/2012

	No Somatostatin	Somatostatin	p-value
Number	295 (58%)	215 (42%)	
Fistula/leak	23 (8%)	7 (3%)	0.031
A	1 (<1%)	2 (1%)	0.999
B	11 (4%)	2 (1%)	0.051
C	10 (3%)	4 (2%)	0.413
B and C	21 (7%)	6 (3%)	0.031
Readmission	30 (10%)	27 (13%)	0.398
LOS	9 (2-81)	9 (2-48)	0.462

Table 2. A comparison of patients receiving prophylactic somatostatin to patients not receiving prophylactic somatostatin

	Univariate	RR	95 % CI	P-value
Somatostatin Use	0.031	0.538	0.180-1.032	0.059
PMH Cardiac	0.002	2.093	1.346-6.082	0.006

Table 3. Multivariate predictors of post-operative pancreatic fistulas

Conclusions

- Somatostatin associated with a statistically significant decrease in both the rate of fistula formation and the number of clinically significant fistulas in our pancreatectomy patients.
- Somatostatin use post-pancreatic resection is beneficial in preventing pancreatic fistulas and improving some post-surgical outcomes.

Results

- Overall, the median length of stay was 9 (2-81) days, 57 (11.2%) patients were readmitted, 215 (42.2%) patients were administered somatostatin, 30 (5.9 %) patients developed postoperative pancreatic fistulas, and 27 (5.3%) fistulas were of clinical significance (grade B or C)
- **Pancreatic fistula developed in 7 (3.3%) patients who received somatostatin versus 23 (7.8%) patients who did not receive somatostatin (p=0.031).**
- **The median length of stay was 9 (2-48) days for patients who received somatostatin versus 9 (1-81) days for those who did not receive somatostatin (p=0.462).**
- **Of the patients who received somatostatin, 27 (12.6%) patients were readmitted versus 30 (10.2%) patients who did not receive somatostatin (p=0.398).**
- **For patients receiving somatostatin, 6 (2.7%) fistulas were of clinical significance versus 21 (7.1%) fistulas for patients who did not receive somatostatin (p=0.031)**
- On multivariate analysis, somatostatin did not reach statistical significance (RR=0.538, CI 95%=0.180 – 1.032, p=0.059)

Acknowledgements

University of Louisville Cancer Education Program NIH/NCI
(R25 CA134283)

Tobacco-Induced Dysregulation of Matrix Metalloproteinases in HL-60 cells.

Black H.M., Renaud D.E., Scott D.A.

Department of Oral Health & Systemic Disease Research,
University of Louisville School of Dentistry, Louisville, Kentucky 40202

Introduction

- Matrix metalloproteinases (MMPs) are a family of approximately 18 secreted and membrane-bound zinc-endopeptidases involved in angiogenesis and tissue remodeling, two key determinants of cancer growth.
- In tumor metastasis, MMPs can break down extracellular components, release bioactive molecules, and induce epithelial-mesenchymal transitions.
- There are distinct correlations between smoking prevalence and cancers such as lung, oral and blood cell cancers.
- Nicotine (3-(1-methyl-2-pyrrolidinyl) pyridine), a key toxic component of tobacco, is thought to dysregulate matrix metalloproteinase secretion in innate immune cells in an α_7 nicotinic acetylcholine receptor (nAChR)-dependent manner.
- HL-60 cells were derived from an individual with acute promyelocytic leukemia and are commonly employed as model of innate immune cell differentiation and function.
- **We set out to examine the influence of nicotine on MMP production by HL-60 cells.**

Materials and Methods

- HL-60 cells were cultured in RPMI 1640 medium in an atmosphere of 5% CO_2 and 100% humidity.
- HL-60 cells were differentiated *(Figure 1)* into neutrophils in by 1.3% DMSO or into monocytes by 16 nM PMA.

Figure 1. Differentiation of HL-60 cells into neutrophilic cells.

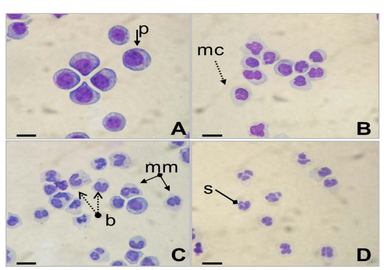

Figure 1: Hema 3 staining of initial differentiating (A) HL-60 cells in 1.3% DMSO then stains over one day (B) three (C), and five (D) days. p: promyelocytes mc: myelocytes; mm metamyelocytes; b: band cells; s: segemented neutrophils.

Figure 2. Expression of Nicotinic Receptors on HL-60 cells

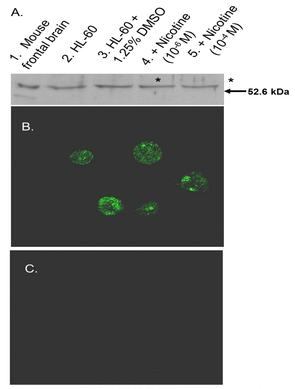

- Promyelocytic and DMSO-differentiated HL-60 cells express α_7-acetylcholine nicotinic receptors (α_7 nAChR).
- (A) α_7 nAChR Western blot. (B) α_7 nAChR Immunofluorescence staining (x1000) (C) Negative control for α_7 nAChR Immunofluorescenc staining (x1000).

Results

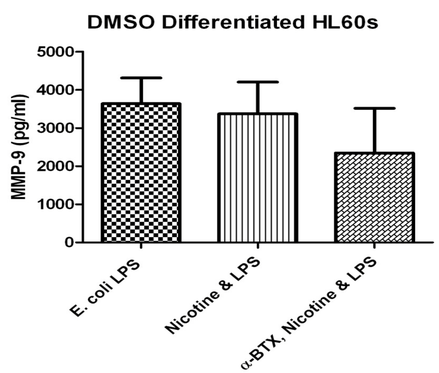

Figure 3. Nicotine does not significantly influence MMP-9 release from LPS-stimulated neutrophilic cells ; α-bungarotoxin (α-BTX) is a α_7 nAChR inhibitor.

Results

Figure 4. Nicotine suppresses LPS-induced MMP-8 release from nicotinic cells.

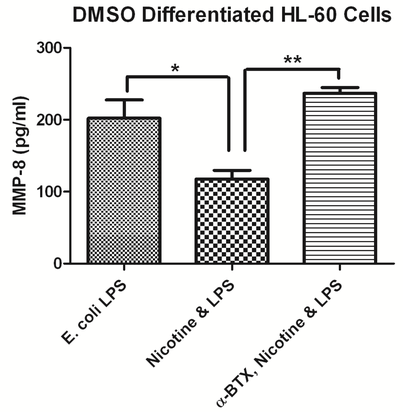

* p< 0.05 and ** p< 0.01

Figure 5. Nicotine does not significantly influence MMP-9 release from LPS-stimulated monocytic cells.

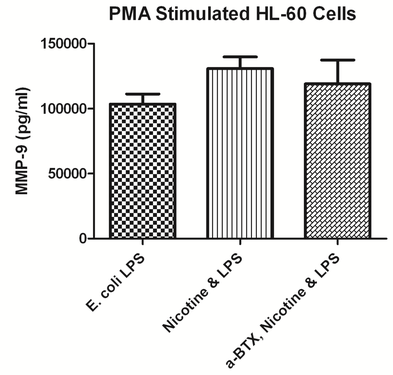

Conclusions

- Nicotine suppressed MMP-8 release from TLR-stimulated neutrophilic HL-60 cells in an α-bungarotoxin-manner.
- Future studies will assess the influence of nicotine on the expression of membrane-bound MMP species as well as MMP expression and secretion in HL-60 cells differentiated into the monocytic lineage.
- The relevance of nicotine exposure to MMP expression and cancer development in innate leukocytes is currently unclear.

Acknowledgements

NCI Cancer Education Program at the University of Louisville, Director: Dr. David Hein (HB)

NIDR R01DEO19826 (DAS)

UNIVERSITY OF LOUISVILLE
It's Happening Here.®

Evaluation of AFP Staging System for Hepatocellular Carcinoma in Non-cirrhotic Patients

Nicolas Burnett, BA, Erik Dunki-Jacobs, MD, Charles Scoggins, MD
Kelly McMasters, MD, PhD, Glenda Callender, MD, Ryan Anderson, BS, Robert CG Martin II, MD, PhD
Department of Surgery, Division of Surgical Oncology, University of Louisville, Louisville, KY

Introduction

- Hepatocellular carcinoma (HCC) is one of the top five most common cancers in the world and one of the top three most common causes of mortality worldwide
- One of the primary staging systems is the Barcelona Clinic Liver Cancer (BCLC) stage based on Child-Pugh score.
- Alpha-fetoprotein (AFP) is used as a biomarker for HCC but until recently its prognostic value remained uncertain.
- In Kentucky, a significant number of patients present without cirrhosis, yet BCLC stage continues to be used to help determine treatment and prognosis.

Purpose of Study

- Determine if BCLC staging was the optimal staging for HCC patients in the South-Midwest given the lack of cirrhosis that they present with.

Methods

- A review of a 4000-patient prospectively collected institutional database was conducted in order to identify patients with HCC.
- Cirrhosis status was determined based on hepatitis serology, history of alcoholism, and CT imaging.
- Data for all patients with a diagnosis of HCC were extracted from the database, including demographics number of liver lesions, extent of liver lesions, pathologic findings of the liver lesion, pathologic findings of the non-neoplastic liver parenchyma, hepatitis serologic test results, AFP level, and outcome.
- Patients were staged using the BCLC staging system as well as the AFP staging system.
- Log-rank tests were performed to compare the 1- and 5-year survival outcomes between stages for each staging system, particularly for the subgroup of non-cirrhotic patients.

Results

Figure 1.

Comparison of cirrhotic vs. non-cirrhotic populations among BCLC stage and AFP stage.

	Cirrhotic	Non-Cirrhotic	p-value
BCLC			0.733
Stage A	145	138	
Stage B	84	78	
Stage C	31	21	
Stage D	7	7	
Stage Unknown	5	2	
AFP			<0.0001
Stage N	58	94	
Stage A	75	57	
Stage B	25	15	
Stage C	77	31	
Stage Unknown	37	49	

Survival All	1 year	5 year	p-value
BCLC			<0.0001
Stage A	82%	46%	
Stage B	66%	26%	
Stage C	60%	20%	
Stage D	61%	0%	
AFP			<0.0001
Stage N	85%	55%	
Stage A	78%	39%	
Stage B	70%	21%	
Stage C	64%	22%	

Survival Non-Cirrhotics	1 year	5 year	p-value
BCLC			0.003
Stage A	76%	43%	
Stage B	64%	21%	
Stage C	53%	24%	
Stage D	86%	0%	
AFP			<0.0001
Stage N	83%	53%	
Stage A	67%	32%	
Stage B	28%	14%	
Stage C	41%	6%	

Figure 2a.

Overall survival at 1 and 5 years for all patients when staged under BCLC system and when staged under AFP system.

Figure 2b.

Overall survival at 1 and 5 years for non-cirrhotic patients only when staged under BCLC system and when staged under AFP system.

Figure 3.

Kaplan-Meier survival curves for all patients separated by BCLC Stage.

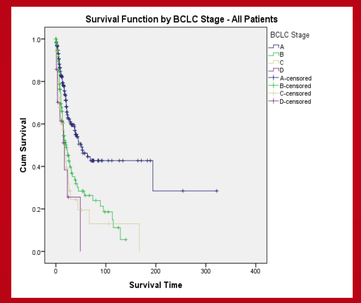

Figure 4.

Kaplan-Meier survival curves for all patients separated by AFP Stage.

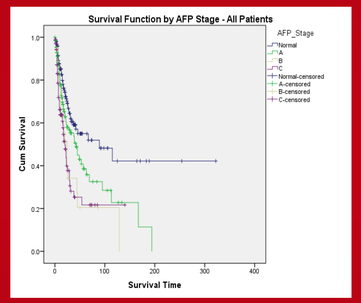

Figure 4.

Kaplan-Meier survival curves for non-cirrhotic patients only separated by BCLC Stage.

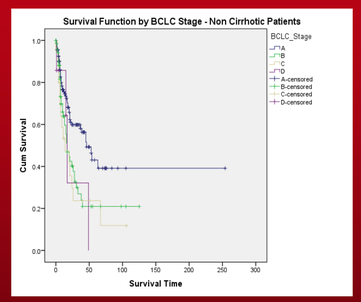

Figure 6.

Kaplan-Meier survival curves for non-cirrhotic patients only separated by AFP Stage.

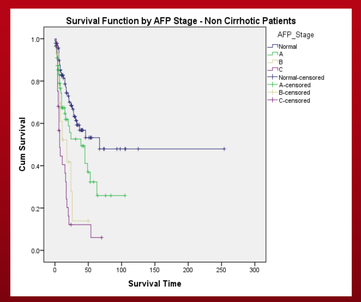

Conclusions

- Patients presenting with HCC in the absence of cirrhosis appear to have different characteristics than patients with cirrhosis. Staging according to AFP level is an appropriate predictor of prognosis in non-cirrhotic patients with HCC.
- While BCLC stage cannot differentiate between cirrhotic and non-cirrhotic patients; AFP stage does. However, both reached statistical significant in predicting overall survival at 1 and 5 years. Neither BCLC stage or AFP stage alone is optimal. Rather, both factors should be taken into account to determine appropriate management for patients.

Results

- A total of 518 patients were included in the study, and the study population was subdivided into cirrhotic (n=272) and non-cirrhotic (n=246) groups
- Median AFP was 58 (range 1-2,520,000) and 10 (range 1-287,004) for cirrhotic and non-cirrhotic patients respectively.
- AFP Stage N (normal) was defined as <10 ng/ml, Stage A as 10-150 ng/ml, Stage B as 150-500 ng/ml, and Stage C as >500 ng/ml as published by Muscari et al
- Chi-square analysis comparing the percent of cirrhotic and non-cirrhotic patients in each BCLC stage was not statistically significant ($p = 0.733$)
- **There was a statistically significant difference between the percent of cirrhotic versus non-cirrhotic patients in each AFP stage ($p < 0.0001$).**
- **There was a statistically significant difference between overall survival of all patients by stage for both the BCLC and AFP systems ($p < 0.0001$ in both cases).**
- **In the non-cirrhotic patient group specifically, there was again a statistically significant difference between overall survival by stage for both the BCLC and AFP systems, although the AFP result had a lower p-value ($p < 0.0001$ for AFP, $p = 0.003$ for BCLC).**

Granulocyte Colony Stimulation Factor (G-csf) Switches Müller Glia from a Gliosis Pathway to a Photoreceptor Progenitor Pathway in Vitro

Laurie Conrad, Guomin Jiang, Yongqing Liu, Henry J. Kaplan, Douglas C. Dean, Wei Wang
Department of Ophthalmology and Visual Sciences
University of Louisville School of Medicine

Introduction

The leading cause of blindness in western countries is retinal degeneration. Loss of photoreceptors leads to permanent vision deficits. In lower vertebrates, Müller glia proliferate in response to retinal damage and dedifferentiate to retinal photoreceptor progenitors, which in turn replace lost photoreceptors. This Müller cell dedifferentiation is triggered by signaling factors which activate the Stat3 transcription factor. In mammals this Müller cell pathway is not significantly activated leaving higher vertebrates susceptible to retinal damage and disease. Here, we investigated the effects of Granulocyte Colony Stimulation Factor (G-csf) on Müller cells in vitro. G-csf is a well known activator of Stat3. It is widely used to boost bone marrow stem cell proliferation and differentiation during chemotherapy. But, recent evidence demonstrates that G-csf has functions beyond its role in chemotherapy—it can stimulate proliferation of cardiac progenitors and neural stem cells to add new differentiated cells to damaged heart and CNS. Moreover, its receptor is expressed on Müller cells in the retina.

Results

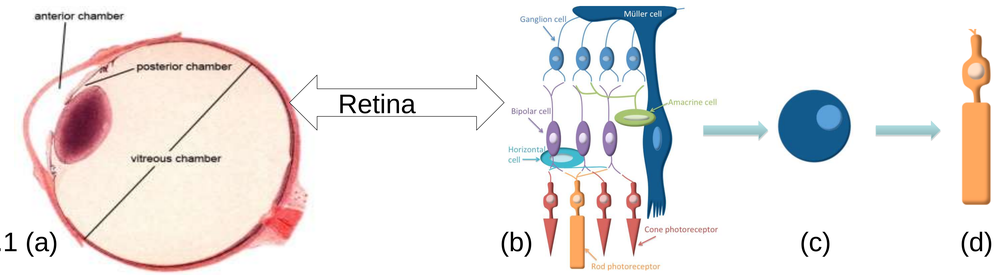

Fig.1. (a) Cross-section of a human eye. The retina is located at the posterior portion of the eye indicated by the arrow. (b) Diagram of cell layers of the retina. (c) Progenitor cell originating from Müller cell in Fig.1(b). (d) Rod photoreceptor differentiated from the progenitor cell in Fig.1(c).

Fig.2

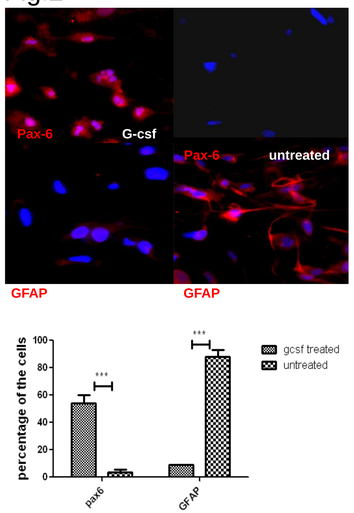

Fig.3

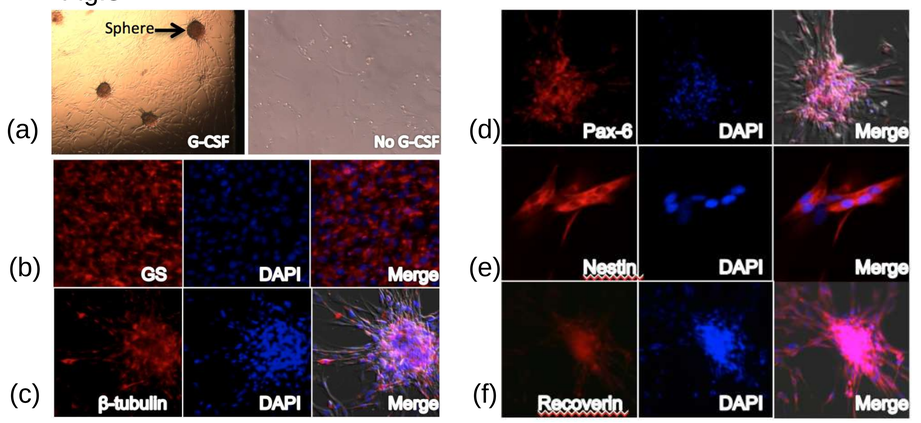

Fig.3 (a) More spheres developed in the G-csf treated group than in the untreated group. (b) Over 90% of cells in culture stained positive for glutamine synthetase (GS), a Müller cell marker. (c-d) After 5 days in culture cells within the spheres stained positive for β-tubulin and pax6, retinal progenitor cell markers. (e) After 5 days in culture cells stained positive for nestin, a retinal progenitor cell marker. (f) After 10 days in culture cells stained positive for recoverin, a photoreceptor marker.

Methods

Mouse Müller cells were cultured on Matrigel in DMEM complete medium with 10% FBS and penicillin/streptomycin. The cells were treated with 100 ng/mg G-csf for 5 or 10 days, then the cells were fixed and immunostained for pax6 (retinal progenitor cells marker), nestin (retinal progenitor cells marker), GFAP (gliosis marker), GS (Müller cells marker), β-tubulin (neuronal cells marker), and recoverin (photoreceptor marker).

Fig.2. G-csf causes an increase in the number of pax6 positive cells and a decrease in the of number of GFAP positive cells. There is significant difference in the percentage of cells with and without these markers between G-csf treated and untreated populations.

Conclusions

Müller glia can progress along two distinct pathways following retinal injury and disease. Cells marked by GFAP contribute to gliosis and retinal damage. Cells in which GFAP is diminished and pax6 and nestin are induced can contribute to cells expressing photoreceptor markers. Our results suggest that G-csf can switch Müller glia from a gliosis pathway to a retinal progenitor pathway.

Acknowledgements

Research supported by grants from Research to Prevent Blindness, National Cancer Institute R25 grant - Cancer Education Program NIH/NCI (R25- CA134283), and the School of Medicine Summer Research Scholar Program.

SUPPORTED BY
Research to Prevent Blindness

BCL6 Expression as a Prognostic Indicator in a Subset of DLBCL.

Noura Estephane[1], Michael W. Gordon[1], Yong Li[1], Ken H Young[2].
[1]Department of Biochemistry and Molecular Biology, University of Louisville School of Medicine
[2]Department of Hematopathology, The University of Texas MD Anderson Cancer Center, Houston TX

Background

Diffuse large B-cell lymphoma (DLBCL) is an aggressive lymphoid neoplasm that accounts for about 40% of all newly diagnosed non-Hodgkin's lymphomas each year. Activated B-cell (ABC) DLBCL possesses gene expression patterns that resemble *in-vitro* activated peripheral B-cells and is characterized by NF-κB activation, while germinal center (GCB) DLBCL shows expression patterns similar to non-malignant germinal center B-cells and carries the better prognosis. *TP53* is a gene coding the tumor suppressor p53, a transcription factor that acts as a sensor of cellular stressors. It functions by regulating various downstream target genes, thus promoting cell cycle arrest, initiating DNA repair, inhibiting angiogenesis, triggering senescence, or initiating apoptosis if cellular damage is irreparable. *BCL6* is a gene coding for a transcriptional repressor that acts in mature GC B-cells through DNA binding and recruitment of co-repressors. It prevents premature activation and differentiation of GC B-cells, and fine-tunes the DNA damage response during somatic hypermutation and class switch recombination. Double-hit B-cell lymphomas are a subset of lymphomas defined by chromosomal breaks involving *MYC* and *BCL2* and carry a poor prognosis. Using a cohort of 506 DLBCL patients including clinical, gene expression and sequencing data, we tested our initial hypothesis that concurrent *BCL6* translocation and *TP53* mutation may also constitute a double-hit lymphoma.

Methods

Gene status and expression percentage was determined by sanger-based sequencing, fluorescence in-situ hybridization (FISH), and immunohistochemistry. Kaplan-Meier survival proportions were determined for various combinations of *BCL6* and *TP53* gene expression and status.

Results

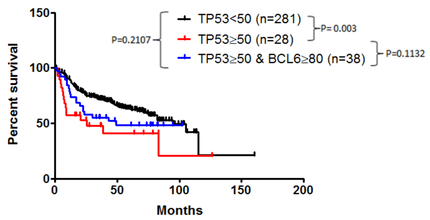

Survival of all patients with wild type p53 expression less than 50%, p53 expression over 50%, and p53 expression over 50% with BCL6 over 80%. (n= 347)

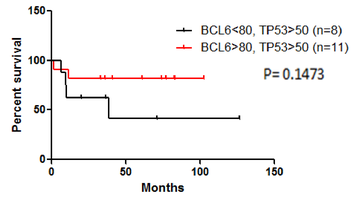

Survival of all patients with wild type p53 expression over 50%, and BCL6 expression over 80%.

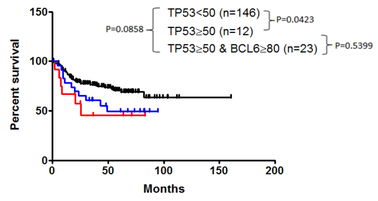

Survival of GCB subtype patients with wild type p53 expression less than 50%, p53 expression over 50%, and p53 expression over 50% with BCL6 over 80%. (n=181)

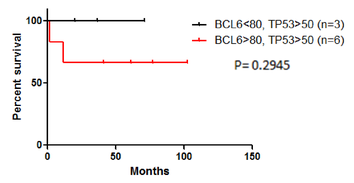

Survival of GCB subtype patients with wild type p53 expression over 50%, and BCL6 expression over 80%.

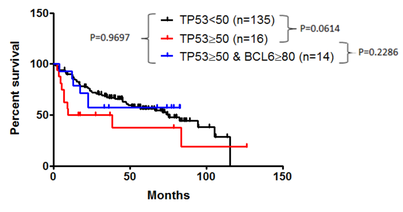

Survival of ABC subtype patients with wild type p53 expression less than 50%, p53 expression over 50%, and p53 expression over 50% with BCL6 over 80%. (n=166)

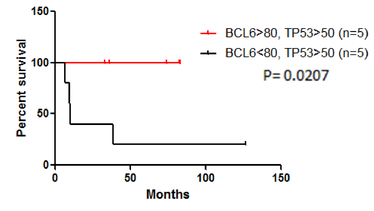

Survival of ABC subtype patients with wild type p53 expression over 50%, and BCL6 expression over 80%.

Conclusions

After analyzing the data of *BCL6* and *TP53* for the potential of a Double-Hit Lymphoma, no significant relationship was found between concurrent mutations and survival. However, we found that in a subset of patients with wild-type but overexpressed *TP53*, expression of *BCL6* may act as a prognostic indicator in ABC-DLBCL but not GCB-DLBCL. Based on Kaplan-Meier analysis, overexpression of *BCL6* in the ABC subtype was found to predict better survival (P=0.0207), while overexpression of *BCL6* in the GCB subtype was found to predict poor survival but was not significant (P=0.2945).

Acknowledgments

I would like to thank Michael Gordon and Yong Li for their help and support throughout this project. I would also like to thank Ken H Young of the Department of Hematopathology at the University of Texas MD Anderson Cancer Center and all the members of the DLBCL consortium.

References

Green TM, Young KH, Visco C, et al: Immunohistochemical Double-Hit Score Is a Strong Predictor of Outcome in Patients With Diffuse Large B-Cell Lymphoma Treated With R-CHOP. Journal of Clinical Oncology, 2012

Basso K: Roles of BCL6 in normal and transformed germinal center B cells. Immunological Reviews 247, 2012

Dalla-Favera R: The BCL6 proto-oncogene suppresses p53 expression in germinal-centre B cells. Nature 432, 2004

Off-Target Drug Effects: The Identification of Natural Products and FDA-Approved Cancer Drugs as G-Quadruplex DNA-Interacting Agents

John D. Gettelfinger[1,3], Huy T. Le[2,3], Lynn W. Deleeuw[1,3], Jonathan B. Chaires[1,2,3], John O. Trent[1,2,3]

[1]Department of Medicine, [2]Department of Biochemistry & Molecular Biology, [3]James G. Brown Cancer Center, University of Louisville, Louisville, KY 40202

Introduction

Guanine-rich oligonucleotide sequences capable of folding into G-quadruplexes, unique quadruple helical tertiary structures, are localized to functionally important sites of the human genome (e.g. the telomere, promoters of oncogenes, and 5'-untranslated and 3'-untranslated regions of several disease-modifying genes). Because of this, G-quadruplexes have emerged as attractive drug targets for cancer and other diseases. In addition to the classical DNA-binding agents (e.g. daunorubicin, distamycin) it is particularly interesting that certain classes of protein-binding agents (e.g. estrogen mimics) have been shown to directly interact with G-quadruplex structures. In the current work, we examined the off-target drug effects of several well-characterized and widely-known compounds by screening the National Cancer Institute Natural Product Set II (120 compounds) and Approved Oncology Drugs Set III (97 compounds) for G-quadruplex-interacting agents.

Methods

Oligonucleotide Preparation and Annealing and Small Molecule Acquisition

The human telomere (hTelo) G-quadruplex sequence with a 6-fluorescein (6FAM) molecule, FRET donor, attached at the 5' end and a tetramethylrhodamine (TAMRA) molecule, FRET acceptor, at the 3' end was obtained from Sigma-Aldrich (St. Louis, MO) and consists of the sequence:

5'-6FAM-AGGGTTAGGGTTAGGGTTAGGG-TAMRA- 3'

Unlabeled hTelo G-quadruplex sequence, polyAT duplex hairpin sequence, and polyGC duplex hairpin sequence were obtained from Integrated DNA Technologies (Coralsville, IA) and consists of the sequences:

5'-AGGGTTAGGGTTAGGGTTAGGG- 3'
5'-ATATATATATCCCCATATATATAT- 3'
5'-GCGCGCGCGCTTTTGCGCGCGCGC- 3'

Stock solutions of the FRET-labeled oligonucleotide (250 μM) and unlabeled oligonucleotides (1000 μM) were made by reconstituting the lyophilized DNA in buffer, which is composed of tetrabutyl ammonium phosphate (10 mM) and EDTA (1 mM), pH 7.0. Prior to annealing, the DNA was further diluted in buffer supplemented with 1 M KCl (final concentration 25 mM) and DMSO (1% v/v). For the initial screening, FRET DNA was diluted to a concentration of 0.4 μM. For the competition experiments, FRET DNA was diluted to a concentration of 0.8 μM while unlabeled DNA was diluted to a concentration of 160 μM. The oligonucleotide samples were annealed in a water bath by heating to 100ºC, holding the sample at temperature for 10 minutes, and gradually cooling to room temperature overnight for the hTelo sequences and cool on ice for 10 minutes for the duplex sequences.

The Natural Product Set II (NPSII) and Approved Oncology Drugs Set III (AODSIII) were obtained from the National Cancer Institute Developmental Therapeutics Program Open Chemical Repository (http://dtp.cancer.gov) in 96-well plate format. NPSII was reconstituted following accompanied instruction while AODSIII was used as obtained. For the melting experiments, compounds were further diluted 100 fold in buffer and supplemented with 1 M KCl (final concentration 25 mM).

Fluorescent Resonance Energy Transfer (FRET) Melting Assay

FRET melting of hTelo was carried out on 96-well plates using Applied Biosystems (Foster City, CA) StepOnePlus PCR System. For the initial screen, annealed FRET-hTelo was mixed with diluted compounds (test) or buffer (control) in a 1:1 ratio. For the G-quadruplex-selectivity screen, annealed FRET-hTelo was mixed with annealed unlabeled DNA and compounds in a 1:1:2 ratio. For all experiments, the reaction volumes was 20 μL. DNA melting was conducted over a temperature range of 20ºC to 98.8ºC with fluorescent readings taken every 0.2ºC. Results were analyzed using Applied Biosystems Proteins Thermal Shift™ Software.

Isothermal Titration Calorimetry (ITC)

ITC was performed using a Microcal VP-ITC microcalorimeter. The unlabeled hTelo was dissolved, dialyzed and annealed in 10 mm tetrabutylammonium phosphate, 1 mM EDTA, 25mM KCl, pH 7.0 to a final concentration of 30μM. Compounds were dissolved in final dialysis buffer to appropriate concentrations. ITC parameters were 10μL injections at 5 minute intervals, reference power 15 μcal/sec, stirring speed 300 rpm. Data processing was performed using Origin 7.0 software supplied with the instrument.

3D Fluorescence Spectroscopy DNA Melt

3D DNA melt was performed on a Jasco FP-6500 Spectrofluorimeter. The FRET-hTelo was diluted from the stock solution to a concentration of 0.25 μM supplemented with KCl and DMSO as previously described. Compounds were prepared as previously described to appropriate concentrations. DNA Melting was conducted over a temperature range of 5ºC to 95ºC with a ramp rate of 1ºC/min. Fluorescence emission spectra (500-650 nm) were collected at various temperatures. The excitation wavelength was 492 nm with maximum emission at 520 nm.

Results

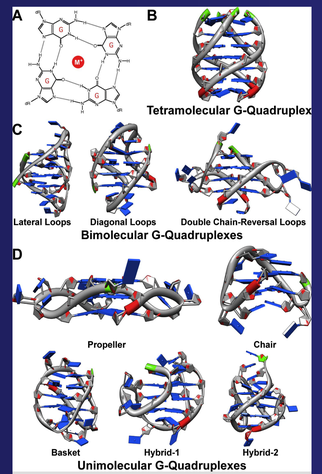

Figure 1. G-quadruplex Structures and Polymorphism

The formation of a G-quartet (a), a square planar arrangement of four guanine bases stabilized by centrally coordinating monovalent cation with Hoogsteen hydrogen bonds between guanine bases, is the first step in the polymorphic formation of G-quadruplex structures (b, c, d). In (b), a tetramolecular G-quadruplex, from four guanine-rich DNA or RNA strands, assumes a parallel topology. In (c), bimolecular G-quadruplexes, from two guanine-rich sequences, can form either a parallel structure with two double chain reversal loops or one of two possible anti-parallel topologies with either two lateral loops or two diagonal loops. In (d), G-quadruplex structures are formed from the folding of a single guanine-rich sequence into a quadruple helical structure that can assume one of several topologies including but not limited to propeller, chair, basket, hybrid-1, or hybrid-2.

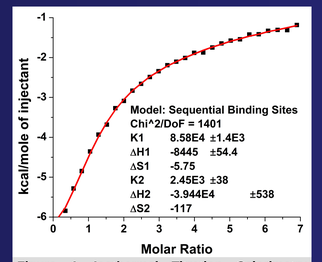

Figure 4. Isothermal Titration Calorimetry Results for Imatinib Binding to hTelo

The binding isotherm is shown for the interaction of 1 mM imatinib to 30 μM hTelo. A sequential binding sites model resulted in the best fit indicating that imatinib binds to hTelo G-quadruplex in a step-wise mechanism where the initial binding of the first imatinib molecule induces a conformational change in the G-quadruplex structure to facilitate the binding of the second imatinib molecule.

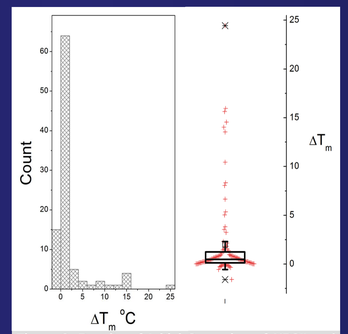

Figure 2. Results of Initial Screening of NPSII and AODSIII against FRET-hTelo

Compounds from the NPSII and AODSIII were screened at 250-fold excess against hTelo using a FRET-based DNA melting assay. The melting temperature (T_m) was determined using the derivative method and was the temperature that corresponded with the maximum of first derivative plot of the melt curve. ΔT_m was calculated by subtracting the T_m of DNA without compound from the T_m of DNA with compound. The distribution of ΔT_m for all compounds is shown. The distribution is represented as a histogram (left). The distribution is shown as a box plot with individual compounds represented as red crosses (right). From the 27 positive hits identified out of the 210 unique compounds screened, the top 12 compounds with the highest ΔT_m, with subtraction of the known classical DNA-intercalators (i.e. daunorubicin, doxorubicin), were selected for additional screening.

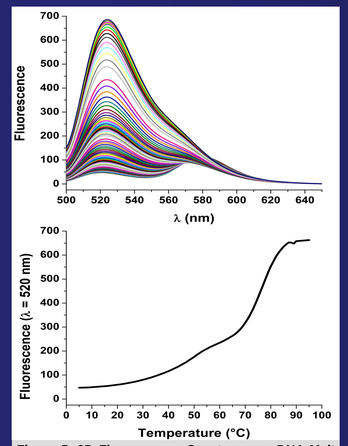

Figure 5. 3D Fluorescence Spectroscopy DNA Melt Demonstrates Imatinib Stabilization of hTelo

FRET-hTelo (0.25 μM) was melted in the presence of imatinib (50 μM) and the fluorescence emission (500-650nm) was monitored during the melt. The fluorescence emission increased with higher temperature (top). The fluorescence emission at 520 nm agreed with previous results from 96-well plate melt experiments (bottom).

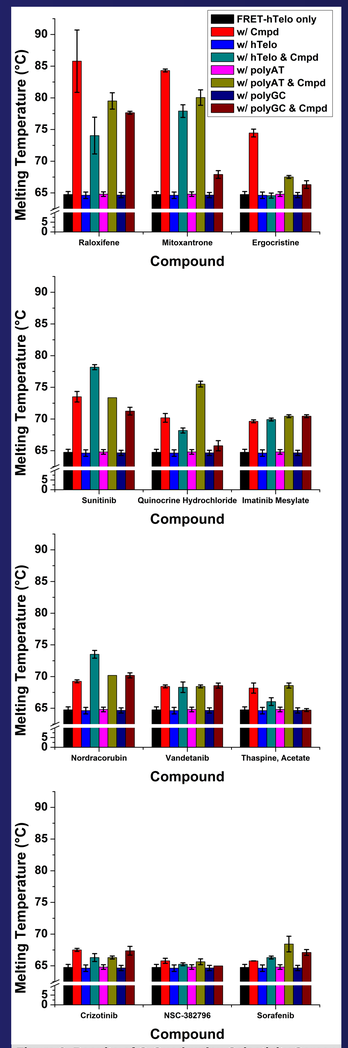

Figure 3. Results of G-Quadruplex-Selectivity Screen

The top 12 G-quadruplex-interacting agents identified from the initial screen was screened for G-quadruplex-selective binding. This was accomplished by the addition of unlabeled DNA to the FRET reaction mixture. The T_m of FRET-hTelo (black) did not change with addition of the unlabeled DNA (blue, pink, navy). Raloxifene, sunitinib, imatinib, crizotinib, sorafenib, nordracorubin, and vandetanib demonstrated selectivity for G-quadruplexes as the T_m in the presence of duplex DNA (tan, maroon) did not decrease significantly compared to FRET-hTelo with no DNA competitor (red) or with unlabeled hTelo (green).

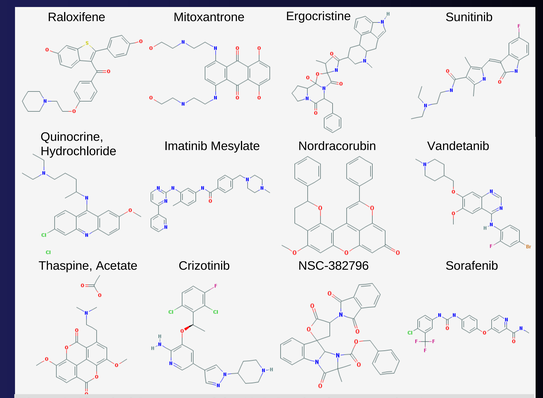

Figure 6. Chemical Structures of the 12 G-Quadruplex-Interacting Agents

Of the 12 G-quadruplex-interacting agents, only 2 compounds (i.e. mitoxantrone, quinocrine) have been previously thought to interact with DNA. Mitoxantrone is a topoisomerase II inhibitor. Quinacrine is a histamine N-methyltransferase inhibitor and was shown in a recent study to bind nonspecifically to DNA. For the other 10 compounds, this study is the first to demonstrate their direct interaction with nucleic acids. From AODSIII, raloxifene is a selective estrogen receptor modulator. Imatinib, sunitinib, vandetanib, crizotinib, and sorafenib are tyrosine kinase inhibitors. Imatinib is particularly important in that it is the first compound to be "rationally designed" for its specific target and is often cited as a model of targeted therapy. From the NPSII, ergocristine is an ergot alkaloid precursor for the hallucinogenic drug lysergic acid diethylamine (LSD). Thaspine is a potential acetylcholinesterase inhibitor. Nordracorubin is a component of Dragon's Blood, an herbal resin mixture that has been used previously as varnish, medicine, incense, and dye. In addition, NSC-382796 is an uncharacterized natural product compound that could serve as a potential precursor for novel small-molecule drugs.

Conclusions

Using a FRET-based melting assay, we were able to identify several novel DNA-binding agents whose actions were previously thought to occur either through an unknown mechanism or through a predominantly protein-binding mechanism. While DNA is a fundamentally attractive drug target, it is often disregarded in drug design and development. As such, DNA is rarely, if at all, considered for off-target drug effects. Of the 27 compounds identified as quadruplex DNA-binding hits from the 210 unique compounds in the initial screen, only 4 had previously been reported as DNA-interactive agents. For the other 28 compounds, this study is the first to demonstrate direct binding interactions between these compounds and DNA. Moreover, 7 of the top 12 compounds exhibited a preference for binding one form of DNA (quadruplex) over another (duplex). Significantly, 5 of the top 12 compounds were tyrosine kinase inhibitors. The observation that many of these drugs, already approved by the FDA, interact with DNA is significant and implies that DNA should be considered for potential off-target effects in drug design and development.

Acknowledgements

Molecular graphics images were produced using the UCSF Chimera package from the Resource for Biocomputing, Visualization, and Informatics at the University of California, San Francisco (supported by NIH P41 RR001081). This work was supported by NIH Grants CA35635 (J.B.C), GM077422 (J.B.C. and J.O.T) and University of Louisville grant, CTSPGP 20058 Award (J.B.C. and J.O.T). J.D.G. was a summer trainee in the Cancer Education Program (supported by NIH/NCI R25 CA134283).